Electronic Supporting Information

for

Heterogeneous interface engineering to enhance oxygen electrocatalytic activity for rechargeable zinc-air batteries

Tao-Tao Li [a], Yu-Rui Ji [a], Yi-Meng Wu [a], Peng-Fei Wang [a], Zong-Lin Liu [a], Jie Shu [b], and Ting-Feng Yi *[a,c,]

[a] *School of Materials Science and Engineering, Northeastern University, Shenyang 110819, PR China*

[b] *School of Materials Science and Chemical Engineering, Ningbo University, Ningbo 315211, PR China*

[c] *Key Laboratory of Dielectric and Electrolyte Functional Material Hebei Province, School of Resources and Materials, Northeastern University at Qinhuangdao, Qinhuangdao 066004, PR China*

[*] **Corresponding author**:

E-mail addresses:

tfyihit@163.com (Ting-Feng Yi)

S1. Materials Characterization

XRD patterns were carried out on a Rigaku instrument with Cu Kα1 radiation. The scanning electron microscopy (SEM) was collected with a Super 55 field emission scanning electron microscope. Transmission electron microscopy (TEM) images, high-resolution TEM (HRTEM) images, and high-angle annular dark field scanning TEM (HAADF-STEM) images were characterized using a Talos F200X transmission electron microscope. X-ray photoelectron spectroscopy (XPS) measurements (XPS, Escalab 250Xi, Thermo Fisher Scientific), with an Al Kα source, were used to interstage the surface properties and compositions of the prepared samples. Raman spectra were carried out at room temperature using a Thermo Fischer DXR via Raman system under Ar^+ (532 nm) laser excitation. The Brunauer-Emmett-Teller (BET) surface area was determined by using an ASAP 2020 instrument. Electron paramagnetic resonance (EPR) spectra were recorded on a Bruker EMX plus spectrometer.

S2. Electrochemical measurements

The electrochemical performance of the samples was measured by using an Ivium VC electrochemical workstation. ORR and OER tests are performed using a three-electrode system in which Hg/HgO electrode is the reference electrode, Pt wire electrode is the counter electrode and the prepared catalyst is the working electrode. The catalyst ink is mainly prepared by ultrasonic mixing of 2.5 mg catalyst, 300 μl DI, 180 μl isopropyl alcohol, and 20 μl Nafion solution. The 6 μl prepared ink was dropped onto the surface of the rotating disk electrode (RDE, d= 3mm) to form a homogeneous

catalytic film, in which the catalyst load was 0.42 mg cm^{-2}. The electrolyte was purged by O_2 gas for at least 30 min before the measurements and the gas flow was maintained during the experiments. Before the ORR measurements, cyclic voltammograms were carried out at 100 mV s^{-1} for at least 20 cycles to clean and stabilize the electrocatalyst surface. Linear scan voltammetry (LSV) measurements were collected at a scan rate of 10 mV s^{-1}. The long-term stability of electrocatalysts was investigated by chronoamperometric responses (CA) and accelerated degradation tests (ADT). Electrochemical impedance spectroscopy (EIS) measurements were conducted in the frequency range from 10^4 Hz to 0.01 Hz with a voltage amplitude of 5 mV. Generally, the applied potential of ORR/OER needs to be converted to a reversible hydrogen electrode (RHE) through the following formula:

$$E(vs.Hg/HgO)+0.59\times pH+0.196 \quad (1)$$

The selectivity of the electrocatalyst during ORR was measured by measuring LSV curves on RDE with different rotating speeds (400, 625, 900, 1225, 1600, 2025, and 2500 rpm). The corresponding electron transfer number (n) was calculated using Koutecky-Levich (K-L) equation:

$$\frac{1}{j}=\frac{1}{j_k}+\frac{1}{j_L}=\frac{1}{B\omega^{1/2}}+\frac{1}{j_k} \quad (2)$$

$$B=0.2nFC_0D_0^{2/3}\upsilon^{-1/6} \quad (3)$$

Where j is the measured current density; j_k and j_L represent kinetic current and limiting current, respectively. And the ω is the rotating rate of the electrode (rpm); n is

the electron transfer number; F is the Faraday constant (96485 C mol^{-1}); C_0 is the bulk concentration of O_2 in the electrolyte (1.2×10^{-6} mol cm^{-3}); D_0, is diffusion coefficient of O_2 (1.9×10^{-5} cm^2 s^{-1}); v is the kinematic viscosity of electrolyte (0.01 cm^2 s^{-1}).

The electron transfer number (n) and hydrogen peroxide yield (H_2O_2%) were calculated from the RRDE measurements according to the following equations:

$$H_2O_2(\%) = 200 \times \frac{\frac{I_r}{N}}{I_d + \frac{I_r}{N}} \quad (4)$$

$$n = 4 \times \frac{I_d}{I_d + \frac{I_r}{N}} \quad (5)$$

Where I_d, I_r, and N are the disk current, ring current, and ring disk electrode collection efficiency (0.42), respectively.

The electrocatalytic OER evaluation was performed in a standard three-electrode system. The catalyst ink was deposited on the working electrode (d=3mm). A Hg/HgO electrode and a carbon rod served as the reference electrode and the counter electrode, respectively. All of the OER measurements were tested at 1 M KOH. The LSV measurements were recorded with a scan rate of 10 mV s^{-1}. The following equation calculated the overpotential (η) of OER:

$$\eta = E_{RHE} - 1.23 \text{ V}. \quad (6)$$

The double layer capacitance (C_{dl}) and electrochemical active surface area (ECSA) of the electrocatalyst were derived from CV curves in the non-Faradic potential region with different scan rates from 20 to 100 mV s^{-1}

S3. Rechargeable Zn-air battery (ZAB) measurements

The prepared catalyst was dripped onto Ni foam as an air cathode, while Zn foil was the anode. The electrolyte consists of 6 M KOH and 0.2 M $Zn(OAc)_2$. The polished zinc foils (0.5 mm thickness). The contact area between the catalyst and electrolyte is 1 cm^2. The mass load of the Co/CoO@N-C-40 catalysts on Ni foam is about 1mg cm^{-2}. In addition, Pt/C and RuO_2 were mixed at a 1:1 molar ratio as reference samples. The polarization curves were collected at a scan rate of 10 mV s^{-1}. The charge/discharge polarisation curves of the ZABs were recorded by the Bio-Logic VPM-300, with the open-circuit voltage as the initial potential and scan rate of 10 m V s^{-1}, corresponding to a power density that multiplies the voltage by the corresponding current density, which allows the determination of the peak power density. The specific discharge capacity was normalized to the mass of the consumed Zn plate based on galvanostatic discharge results. The galvanostatic discharging-charging evaluation was conducted with a NEWARE multichannel battery instrument.

S5. Additional Figs in supporting information

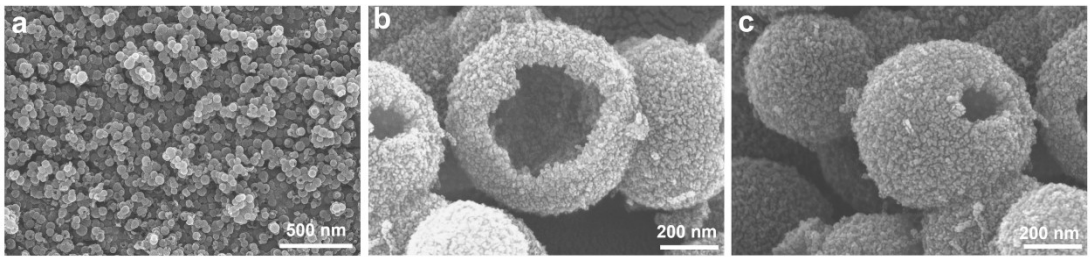

Fig. S1. (a-c) SEM images of Co@N-C-20.

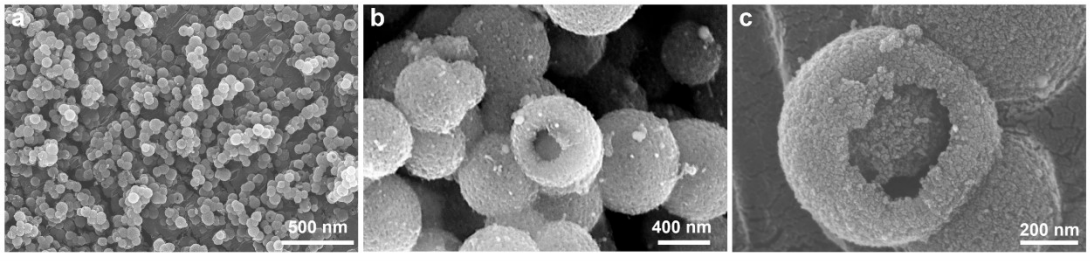

Fig. S2. (a-c) SEM images of Co@N-C-60.

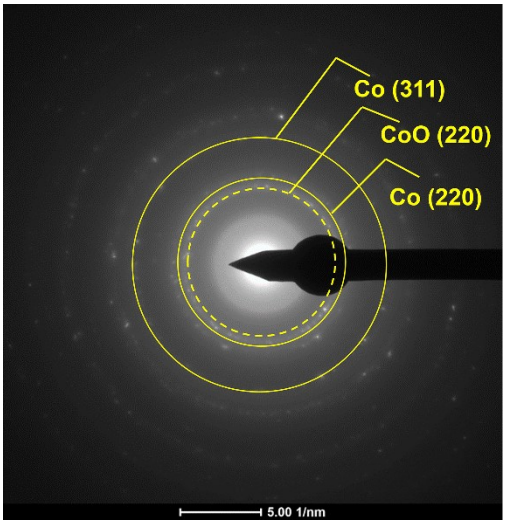

Fig. S3. SAED pattern of Co/Co@N-C-40.

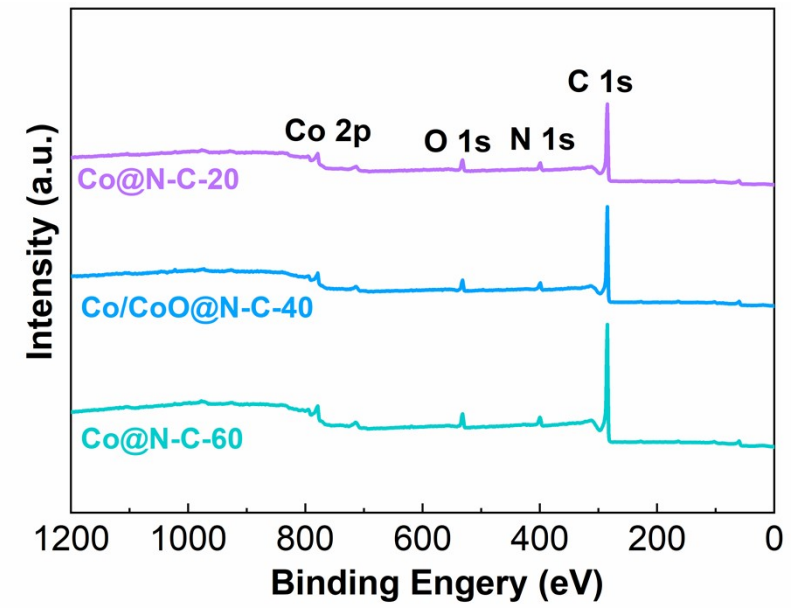

Fig. S4. The XPS survey spectra.

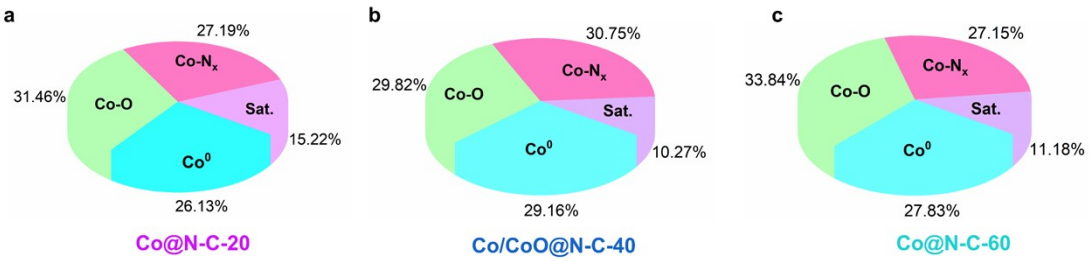

Fig. S5. Content of Co species for Co@N-C-20, Co/CoO@N-C-40, and Co@N-C-60.

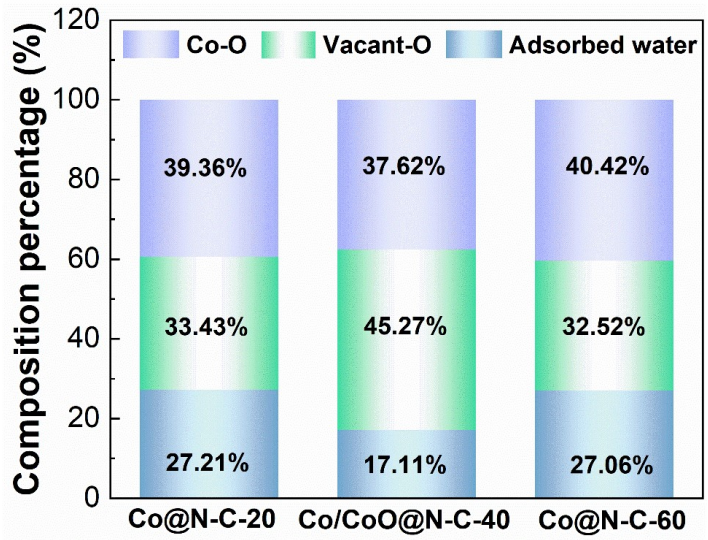

Fig. S6. Content of O species for Co@N-C-20, Co/CoO@N-C-40, and Co@N-C-60.

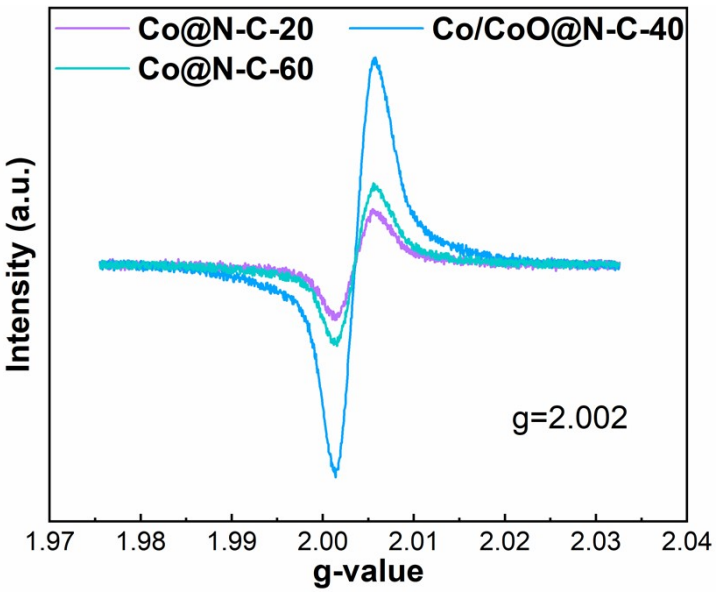

Fig. S7. EPR spectra of Co@N-C-20, Co/CoO@N-C-40 and Co@N-C-60

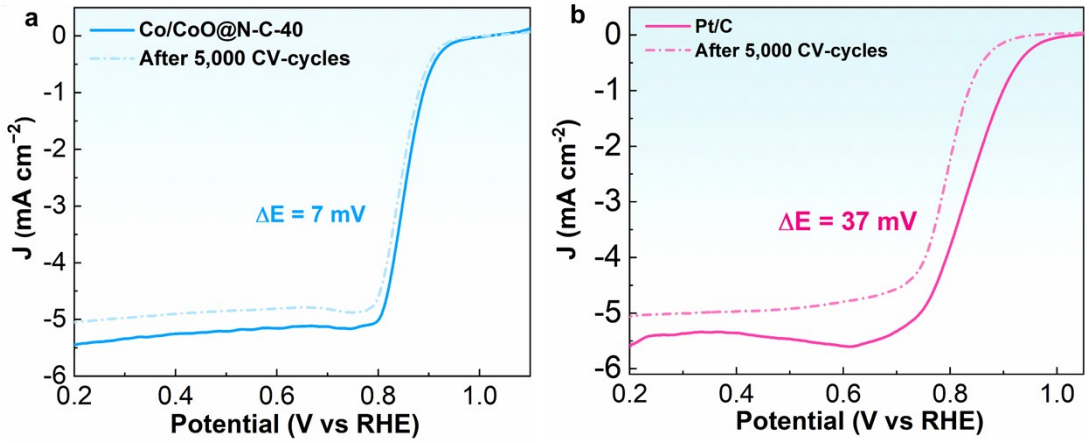

Fig. S8. ORR polarization curves of (a) Co/CoO@N-C-40 and (b) Pt/C before and after 5,000 CV cycles.

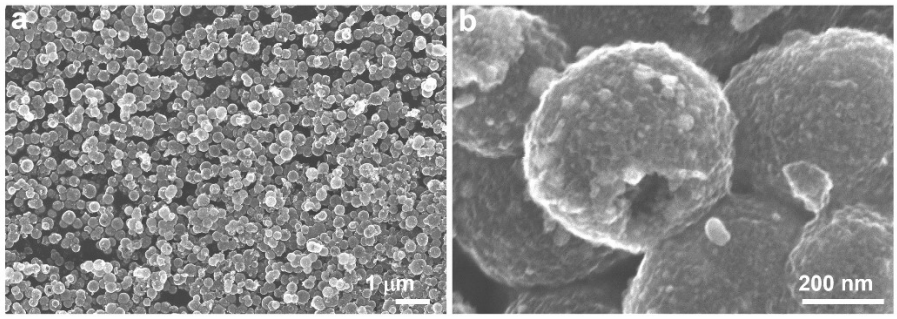

Fig. S9. (a, b) SEM images of Co/CoO@N-C-40 after 5, 000 CV cycles in 0.1 M KOH.

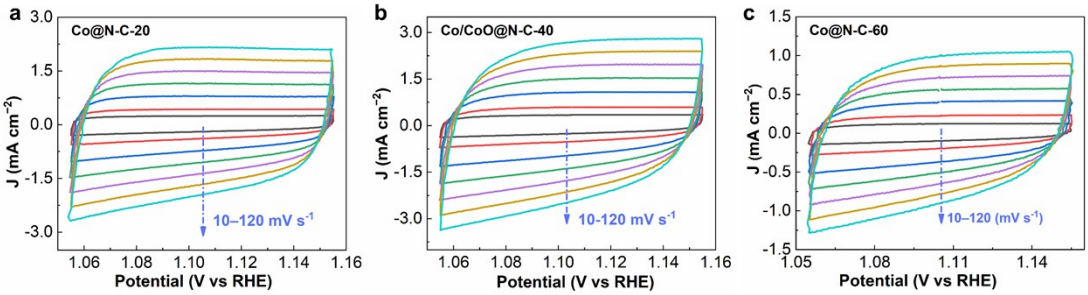

Fig. S10. CV curves of (a) Co@N-C-20, (b) Co/CoO@N-C-40, (c) Co@N-C-60 in 1.0 M KOH.

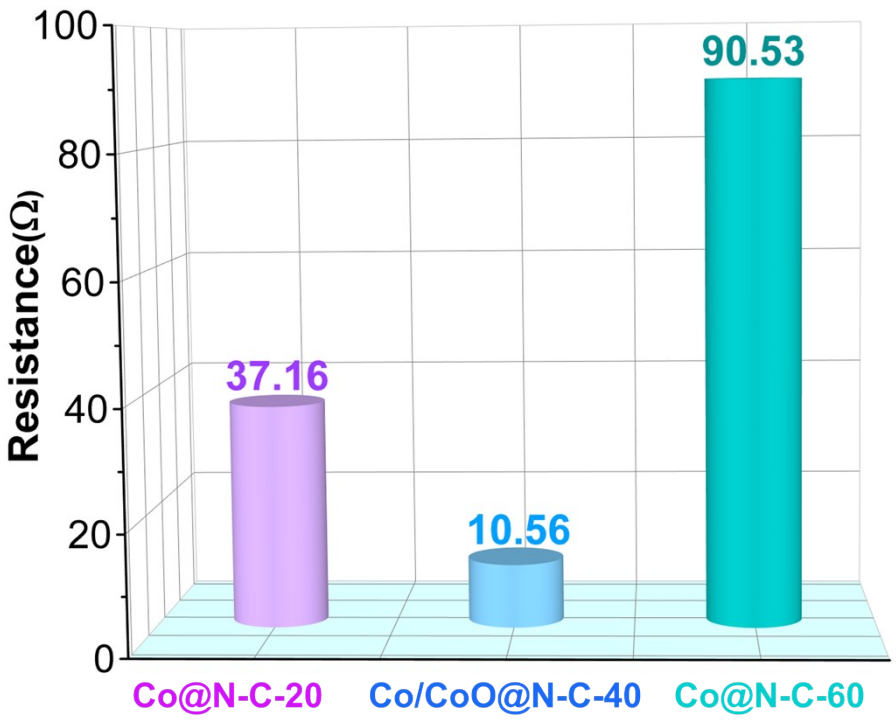

Fig. S11. The value of R_{ct} for Co@N-C-20, (b) Co/CoO@N-C-40, (c) Co@N-C-60.

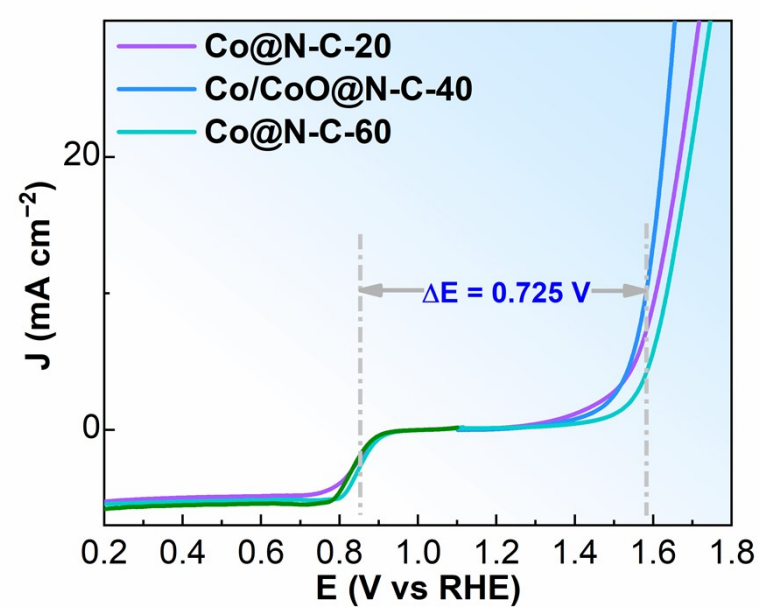

Fig. S12. Bifunctional catalytic activities of electrocatalysts toward ORR and OER.

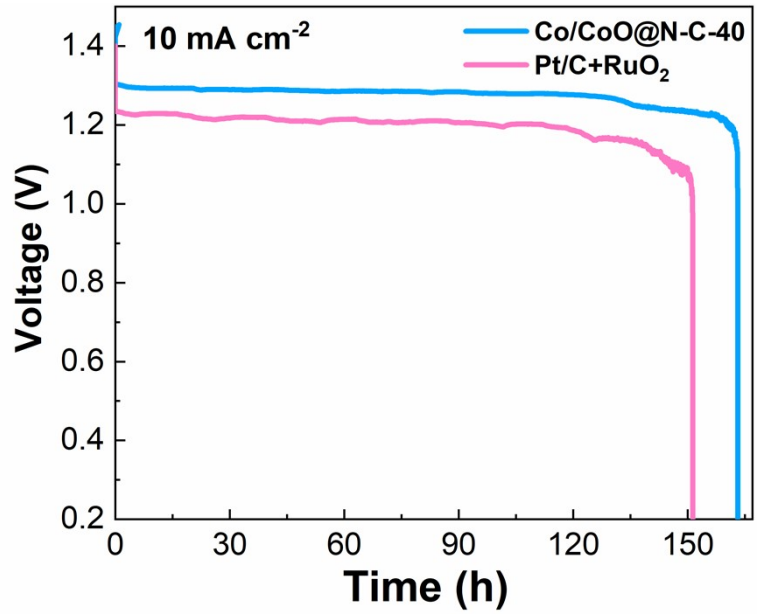

Fig. S13. Discharge performance of ZABs based on Co/CoO@N-C-40 at 10 mA cm^{-2}.

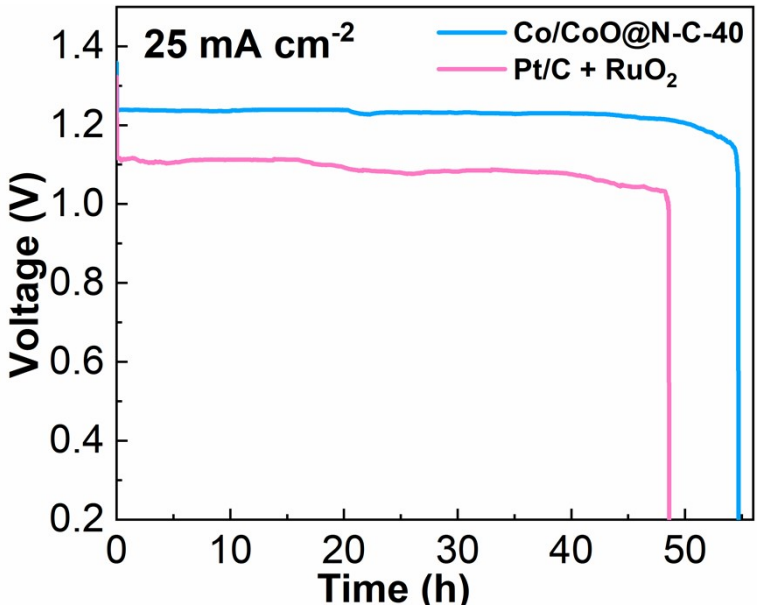

Fig. S14. Discharge performance of ZABs based on Co/CoO@N-C-40 at 25 mA cm^{-2}.

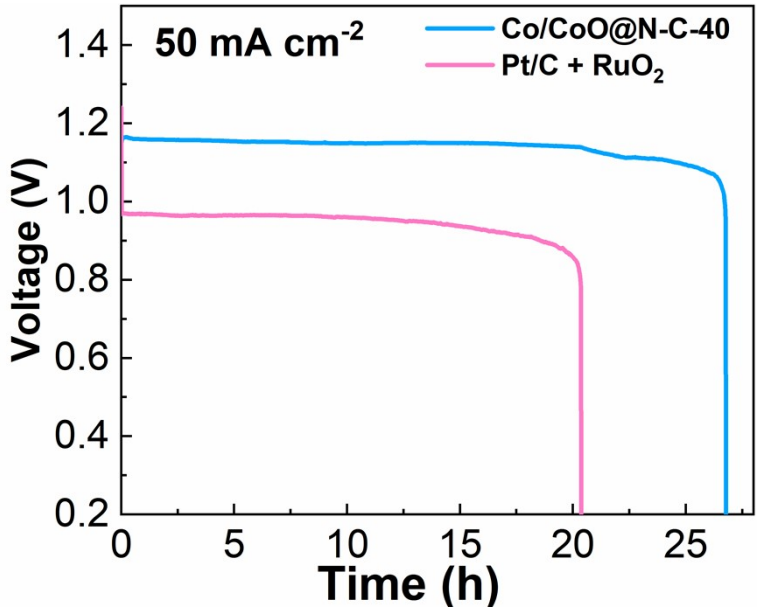

Fig. S15. Discharge performance of ZABs based on Co/CoO@N-C-40 at 50 mA cm^{-2}.

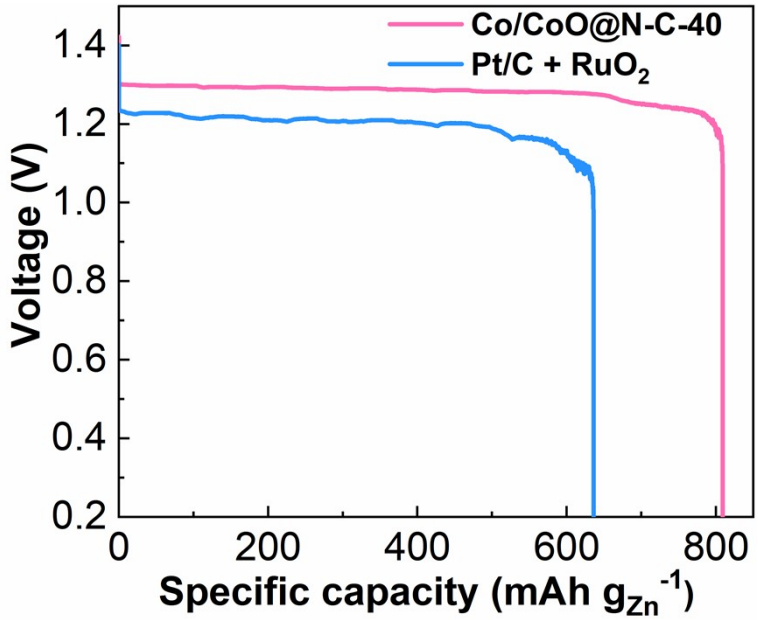

Fig. S16. Specific capacity curves at 10 mA cm^{-2}

S6. Additional tables in supporting information

Table S1. Elemental analysis results.

Sample	C (wt%)	N (wt%)	Co (wt%)	O (wt%)	Zn (wt%)
Co@N-C-20	83.5	7.05	2.41	6.74	0.30
Co/CoO@N-C-40	85.63	6.33	2.18	5.54	0.32
Co@N-C-60	86.33	6.21	2.22	5.22	0.02

Table S2. Summary of performance based on Co-N-C-40 and non-precious metal catalysts for liquid RZABs with alkaline electrolyte (6.0 M KOH + 0.2 M $Zn(OAc)_2$).

Catalysts	OCV (V)	Power density (mW cm^{-2})	Specific capacity ($mAhg^{-1}$)	Cycle time (h)	Ref.
Co/CoO@N-C-40	1.47	186	808@10 mA cm^{-2}	750@10 mA cm^{-2}	This work
$PMnCo_2O$@PWC	1.57	160	811.3 @100 mA cm^{-2}	400@10 mA cm^{-2}	1
$Mn_{0.3}Ru_{0.7}O_2$	/	179	812@10 mA cm^{-2}	800 h@10 mA cm^{-2}	2
Co/SP-NC	1.46	187	801@10 mA cm^{-2}	280@10 mA cm^{-2}	3
CoSe2 @NC	1.45	137	751@10 mA cm^{-2}	167@10 mA cm^{-2}	4
SA-Co-N_4-GCs	1.51	149	600@10 mA cm^{-2}	167@5 mA cm^{-2}	5
Sn SA/OCNTs	1.5	105	786@10 mA cm^{-2}	200@2 mA cm^{-2}	6
$MnCo_2O_4$/NCNTs	1.46	74	827@5 mA cm^{-2}	100@5 mA cm^{-2}	7
FeMn-N-C	1.49	151	795@50 mA cm^{-2}	700@10 mA cm^{-2}	8

$Fe_{1.2}(CoNi)_{1.8}S_6$	1.45	224.8	808@10 mA cm^{-2}	140@10 mA cm^{-2}	9
CoP/FeP@PCN	1.52	175	750@5 mA cm^{-2}	600@5 mA cm^{-2}	10
$FeNi_{jns}$/NC	1.44	210	742@10 mA cm^{-2}	140@5 mA cm^{-2}	11
SA-Fe-SNC@900	1.46	218	798.@5 mA cm^{-2}	200@5 mA cm^{-2}	12
Co_2P/CoN_4@NSC-500,	1.40	103	770@5 mA cm^{-2}	183@5 mA cm^{-2}	13

Reference

1. Y. Liu, S. Liu, P. Zhang, J. Zhou, H. Liu, S. Li, X. Li, X. Wang, D. Han, Y. Chen, Y. Wang, J. Jiang and B. Li, Electronic structure regulation of $MnCo_2O_4$ via surface-phosphorization coupling to monolithic carbon for oxygen electrocatalysis in Zn-air batteries, *Adv. Funct. Mater.*, 2024, 2400522.
2. T. Zhou, W. Wang, H. Luo, Y. Wu, R. Xia, Y. Zhang, Z. Li, G. Jia, T. Zhang, H. Peng and Z. Guo, Asymmetrical Ru–O–Mn bridge active sites fully decouple bifunctional oxygen electrocatalysis for rechargeable zinc-air batteries, *ACS Catal.*, 2024, **14**, 9313-9322.
3. H. Chang, X. Liu, S. Zhao, Z. Liu, R. Lv, Q. Zhang and T.F. Yi, Self-assembled 3d N/P/S-tridoped carbon nanoflower with highly branched carbon nanotubes as efficient bifunctional oxygen electrocatalyst toward high-performance rechargeable Zn-air batteries, *Adv. Funct. Mater.*, 2024, **34**, 2313491.
4. K. Ding, J. Hu, J. Luo, W. Jin, L. Zhao, L. Zheng, W. Yan, B. Weng, H. Hou and X. Ji, Confined n-cose2 active sites boost bifunctional oxygen electrocatalysis for rechargeable Zn–air batteries, *Nano Energy*, 2022, **91**, 106675.
5. N. Yu, H. Chen, J. Kuang, K. Bao, W. Yan, J. Ye, Z. Yang, Q. Huang, Y. Wu and S. Sun, Efficient oxygen electrocatalysts with highly-exposed Co-N_4 active sites on N-doped graphene-like hierarchically porous carbon nanosheets enhancing the performance of rechargeable Zn-air batteries, *Nano Res.*, 2022, **15**, 7209-7219.
6. X. Shao, R. Gan, Y. Rao, T. T. T. Nga, M. Liang, C.L. Dong, C. Ma, J. Y. Lee, H. Li and H. Lee, Main group SnN_4O single sites with optimized charge distribution for boosting the oxygen reduction reaction, *ACS Nano*, 2024, **18**, 14742-14753.
7. Z. Wang, J. Huang, L. Wang, Y. Liu, W. Liu, S. Zhao and Z. Q. Liu, Cation-tuning induced d-band center modulation on co-based spinel oxide for oxygen reduction/evolution reaction, *Angew. Chem. Int. Edit.*, 2022, **61**, e202114696.
8. C. Hu, G. Xing, W. Han, Y. Hao, C. Zhang, Y. Zhang, C.H. Kuo, H.-Y. Chen, F. Hu, L. Li and S. Peng, Inhibiting demetalation of Fe-N-C via Mn sites for efficient oxygen reduction reaction in zinc-air batteries, *Adv. Mater.*, 2024, 2405763.
9. H. Wu, Z. Li, Z. Wang, Y. Ma, S. Huang, F. Ding, F. Li, Q. Zhai, Y. Ren, X. Zheng, Y. Yang, S. Tang, Y. Deng and X. Meng, Regulation of electronic structure in medium-entropy metal sulfides

nanoparticles as highly efficient bifunctional electrocatalysts for zinc-air battery, *Appl. Catal. B*, 2023, **325**, 122356.

10. K. Chen, L. Wang, J. Long, F. Zhao and L. Kang, Petaloid CoP/FeP composites: Efficiently bifunctional cathode electrochemical oxygen catalysts for aqueous and solid-state zinc-air batteries, *Chem. Eng. J*, 2024, **496,** 153820.
11. X. Liu, F. Zhao, L. Jiao, T. Fang, Z. Zhao, X. Xiao, D. Li, K. Yi, R. Wang and X. Jia, Atomically dispersed Fe/N_4 and Ni/N_4 sites on separate-sides of porous carbon nanosheets with Janus structure for selective oxygen electrocatalysis, *Small*, 2023, **19**, 2300289.
12. Z. Chen, X. Peng, Z. Chen, T. Li, R. Zou, G. Shi, Y. Huang, P. Cui, J. Yu, Y. Chen, X. Chi, K. P. Loh, Z. Liu, X. Li, L. Zhong and J. Lu, Mass production of sulfur-tuned single-atom catalysts for Zn–air batteries, *Adv. Mater.*, 2023, **35**, 2209948.
13. Q. Lu, J. Yu, X. Zou, K. Liao, P. Tan, W. Zhou, M. Ni and Z. Shao, Self-catalyzed growth of co, n-codoped CNTs on carbon-encased CoS_x surface: A noble-metal-free bifunctional oxygen electrocatalyst for flexible solid Zn-air batteries, *Adv. Funct. Mater.*, 2019, **29**, 1904481.